ISBN: 978-989-98836-3-5
UNIVERSIDADE DE ÉVORA
INSTITUTO DE INVESTIGAÇÃO
E FORMAÇÃO AVANÇADA

UNIVERSIDADE DE ÉVORA Online Workshop on Earth and Space Sciences - Atmospheric Physics and Climate 2020

Online Workshop on Earth and Space Sciences - Atmospheric Physics and Climate

Proceedings Book
2020

PhD Program in Earth and Space Sciences

Universidade de Évora

UNIVERSIDADE DE ÉVORA
INSTITUTO DE INVESTIGAÇÃO
E FORMAÇÃO AVANÇADA

ONLINE WORKSHOP ON EARTH AND SPACE SCIENCES - ATMOSPHERIC PHYSICS AND CLIMATE

Proceedings Book 2020

within the curricular unit Seminar I (Physics of Atmosphere and Climate) of the

PhD program in Earth and Space Sciences

Universidade de Évora

Instituto de Investigação e Formação avançada e

Departamento de Física

Editors:
Maria João Costa
Rui Salgado

Title: ONLINE WORKSHOP ON EARTH AND SPACE SCIENCES - ATMOSPHERIC PHYSICS AND CLIMATE
Coordinators: Maria João Costa e Rui Salgado
Editors: Maria João Costa e Rui Salgado
June 2020

Rua Romão Ramalho, 59
7000-671 Évora Portugal
ISBN: 978-989-98836-3-5

Indice

Preface

This book was produced in the scope of the Curricular Unit Seminar I (Physics of Atmosphere and Climate) of the PhD program in Earth and Space Sciences, which included the organization of the 2020 edition of the Online Workshop on Earth and Space Sciences - Atmospheric Physics and Climate of the University of Évora. This volume brings together the research articles produced by students who attended the course. Since its first edition in 2013, the Workshop has been a space for sharing knowledge and training in science communication. In this sense, it seeks to provide students who attend Seminar Units with an effective experience not only in the preparation and presentation of oral communications and research articles, but also in the organization of the event itself. In the 2020 edition, which took place on June 4, 11 abstracts were submitted and presented, covering the various themes of the PhD program, in addition to two invited lectures.

Évora, 7 October 2020

Maria João Costa and Rui Salgado
Lecturers of the Curricular Unit Seminar I
(Physics of Atmosphere and Climate)

Acknowledgement

The professors of the Curricular Unit Seminar I (Physics of Atmosphere and Climate) of the Doctoral program in Earth and Space Sciences express their recognition to the authors of the published works. Special thanks to the supervisors who accompanied the students, an action that greatly strengthened the scientific quality of the works presented here.

We thank the support of the Institute for Research and Advanced Training (IIFA) and the School of Science and Technology (ECT) of the University of Évora in publicizing the event.

ONLINE WORKSHOP ON EARTH AND SPACE SCIENCES ATMOSPHERIC PHYSICS AND CLIMATE

4TH OF JUNE, 2020, 11:00 (GMT+1)

HTTPS://VIDEOCONF-COLIBRI.ZOOM.US/MEETING/REGISTER/TJEUFUGGQT8TGNZRICPLDEZSAAPWIVNW8ZUS

MORNING SESSION

11:00 – 11:30	Pedro Matos Soares (invited speaker)	Climate change: from global to regional scales
11:30 – 11:45	Ana Galveias	Effect of meteorological parameters on Cupressaceae pollen in southwestern Iberia
11:45 – 12:00	Fahad Faisal	A comparative review on cooling techniques to develop hybrid PV/T panel
	COFFEE BREAK	
12:15 – 12:30	Carla Lisci	Building pathology: some case studies and decay prediction
12:30 – 12:45	João Perdigão	Direct Normal Irradiance Forecasts based on IFS/ECMWF in the south of Portugal
12:45 – 13:00	Ines Hamak	Three-dimensional crustal image of Arraiolos aftershock sequence, earthquake of M=4.9 (2018), in Central Portugal
	LUNCH BREAK	

AFTERNOON SESSION

Dina Santos (invited speaker)	Operational aeronautic meteorology	14:30 – 15:00
Jebun Naher Sikta	Optomechanical design and integration of a space telescope, for a LIDAR	15:00 – 15:15
Edgar Abreu	Developing a model to determine circumsolar irradiance under clear-sky conditions	15:15 – 15:30
	COFFEE BREAK	
Gonçalo Rodrigues	Satellite remote sensing of water quality parameters over a large reservoir	15:45 – 16:00
Yufan Ding	Novel aseismic structure design - metamaterials	16:00 – 16:15
André Albino	Modelling and studies of the spectral response of some optoelectronic components	16:15 – 16:30
Sara Pereira	Prediction of solar resource and photovoltaic energy production through the generation of a Typical Meteorological Year and Meso-NH simulations	16:30 – 16:45

UNIVERSIDADE DE ÉVORA
INSTITUTO DE INVESTIGAÇÃO E FORMAÇÃO AVANÇADA

ICT Instituto de Ciências da Terra Institute of Earth Sciences

PhD in Earth and Space Sciences
Seminário I - Física da Atmosfera e do Clima

A COMPARATIVE REVIEW ON COOLING TECHNIQUES TO DEVELOP HYBRID PV/T PANEL

FAHAD FAISAL

Department of Physics, University of Évora, R. Romão Ramalho 59, 7000-671 Évora, Portugal, d44773@alunos.uevora.pt

MOUHAYDINE TLEMÇANI

Lithosphere Dynamics Group, Instrumentation Lab, R. Romão Ramalho 59, 7000-671 Évora, Portugal, tlem@uevora.pt

Renewable energy will be the leading source of power on the upcoming days. Solar irradiation is one of the most convenient sources due to abundance in nature. Right now scientist are facing challenges to mitigate the heat induced by the solar panel during the conversion process. Excessive heat degrades the electrical property of photovoltaic panel thus resulting in reduced efficiency. To improve the efficiency different cooling techniques have been introduced namely active and passive cooling. It is really important to select the right cooling technique while developing the PV panel. It is found that, passive cooling technique is more preferable in-terms of operating cost, ease of use and reliability.

1 Introduction

Day by day the demand for electricity is increasing to meet the demand of increased population of this world. We can not think of a single moment without electricity. The electric power generation system is mostly dependent on fossil fuel till date. But this source will not able to meet the future demand if the consumption is continued in the same way or more. Scientist are working day and night to find some alternative sources of energy. Right now all the researchers are focusing on renewable energy which is considered as the ultimate source of eco-friendly energy. The main benefit of solar energy is- it is abundant in nature and completely free in terms of cost. Although challenges are there to store the solar energy. Solar irradiation is converted into power with the help of photovoltaic (PV) solar panel which is the intermediate medium of the whole conversion process. There exist some limitations as well. It is not capable of converting the whole irradiation into power. Till now the maximum efficiency of a panel reached around 25.6% [1] which is very low. The main reason behind this is the solar irradiation does not fall into the solar panel uniformly throughout the day as the incident angle varies during the whole period. Apart from that, the peak time when solar irradiation is in parallel with the panel- it produces a lot of heat as well on the panel which decreases the electrical property of the panel thus resulting in reduced power generation. By thumb of rule for the increase of each 10°C the efficiency of the panel decreases by 5% [2]. Scientist are working day and night to increase the efficiency of the panel by introducing new manufacturing materials, techniques and off-course by optimizing the existing available methods. It is found that- we can keep the existing panel in a stable condition during the peak hour when the conversion is hampered due to additional heat by applying some cooling techniques. Cooling techniques are divided into two types namely: active cooling technique and passive cooling technique. Here we will be comparing both of the techniques with their

possible advantage and disadvantage to implement a photovoltaic thermal (PVT) solar panel. The whole paper will be focused on the improvement of thermal panel.

2 Background study

As we discussed earlier, there are two types of cooling technique involved while dealing the thermal PV panel system. The active cooling technique requires external power to reduce the heat level by spraying fluids on the surface, blowing air through the panel or passing through fluids on the back side of the panel using motor pump. On the other hand passive technique does not require any external power. It is always on the first choice of the researchers due to low operational cost, eco-friendliness followed by high reliability. Here all the techniques involved for active and passive cooling will be discussed with their possible pros and cons.

2.1 *Active cooling techniques*

In general the cooling process related with thermal panel can be categorized in the following way shown in Figure-1:

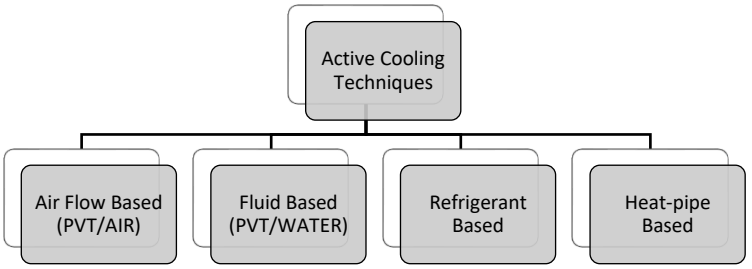

Figure 1. Different cooling techniques

Air based cooling technique: It is one of the most popular non-expensive technique used in thermal PV panel to reduce the heat. The main concept is to create a channel between the solar cell and the back wall via which air can pass through. While designing the air based cooling system two parameter should be taken into consideration namely channel depth and mass flow rate. Channel depth should be at 10 cm to obtain the optimum results [3]. Although it is considered that for efficient heat extractions use of thin (flat) metallic sheet (TMS) in the middle of the channel or adding fins at the back wall of the channel could be more effective for faster heat dissipation comparing with the traditional one which is shown in Figure 2. The energy performance of any PV panel can be determined from the following Eq. (1):

$$Electrical\ Efficiency,\ \eta_{pv} = \eta_{ref}(1 - \beta(T_{pv} - T_{ref})) \quad \text{Eq. (1)}$$

Here,

$\eta_{ref} = reference\ efficiency$

$\beta = cell\ efficiency\ temperature\ coefficient$
$T_{ref} = Standard\ Temperature\ (25°C)$
$T_{pv} = Operating\ temperature\ of\ the\ module$

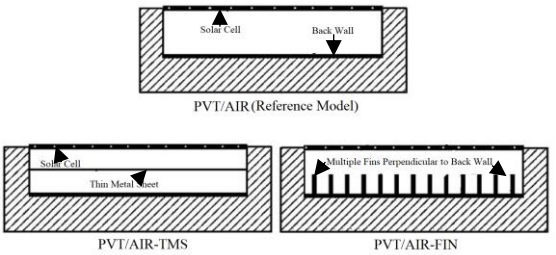

Figure 2. Different cross sectional view of PVT/AIR model

For any weather condition η_{ref} can be determined with temperature ranging from 20°C to 70°C from the relation curve between electrical efficiency and panel temperature.

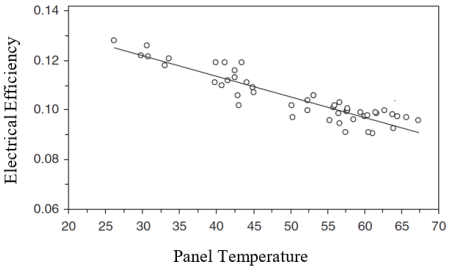

Figure 3. Relation between electrical efficiency and panel temperature

In a natural air flow condition a maximum efficiency of 12.5% is achieved [4].

Fluid based cooling technique: Till now fluid based cooling technique is considered as the most efficient way which includes regular water and different kinds of concentrated fluids (combination of different chemical composition) as it has high capability of heat absorption. For example, by spraying water on top of the surface panel using nozzle- a reduction of temperature between 10 -15 ℃ is achieved [5]. In addition to that, the above mentioned method cleans the panel surface thus resulting in 2-3.5% reduced reflection loss. Water trickling method is applied on top of the surface which

increases the system output almost 15% as the heat is dissipated due to convection process between the water and panel [6]. This method is capable of reducing the operating temperature upto 50% which is really promising. Recently a technology is widely accepted which is based functionally graded materials (FGM's). This cooling technique involves, a gradation of materials from metal dominated layer to other material layer (polymer). Water tubes are included on top part of the panel which have high thermal conductivity for heat dissipation in all direction [7] which is shown in Figure 4. In this way higher efficiency of 12.3% is achieved at lower temperature like 35°C.

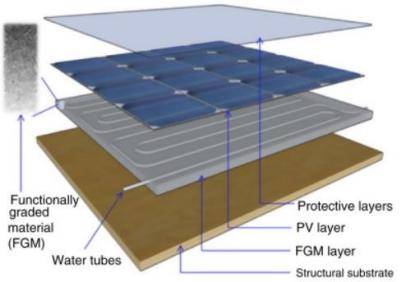

Figure 4. FGM layer [7]

As we can see from the picture that FGM layer functions as an intermediate layer for heat dissipation and suitable for domestic use with rooftop solar system.

Refrigerant based cooling technique: This method is still under test and not suggested as it has some technical limitations. The main concept is to pass the refrigerant through pipes beneath the solar cell where the additional heat will be evaporated which is shown in Figure 5. In this case a very well maintained control system is required to ensure the pressure level of the

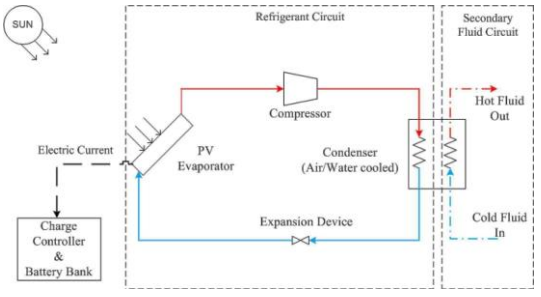

system. In general it is very expensive with high probability of getting damage

due to leakages. This technique along with heat pipe based method is not recommended due to their limitations.

Figure 5. Refrigerant circuit [8]

2.2 *Passive cooling techniques*

Passive cooling technique does not involve any external sources like active cooling technique thus resulting in low operating cost, low maintenance, high reliability and more eco-friendly in nature. There are different ways to apply passive cooling on the panel. Major technique involves - i) submerged water cooling, ii) heat sink, iii) phase changed materials (PCM), iv) cotton wick cooling, v) evaporative cooling and vi) using dielectric medium.

Submerged water cooling: In this method the flat PV panel is submerged in shallow water. The performance is studied by setting different levels (0-10 cm) of water. Although challenges are there as the solar spectrum is different in water. This method results in an increase of power upto 15%. From the final result- it is found that maximum conversion efficiency is achieved at a depth of 4 cm. The performance of the panel varies a lot during different season of the year as the ambient temperature is not same all the time [9].

Heat sink: In this method some fins (mostly aluminum plated) are attached on the back side of PV panel with the help of adhesive. This technique functions well when there is a significant difference in temperature between the sink and ambient air to transfer the heat. With the help of this technique a decrease of minimum 25-30°C in temperature is achieved. Although proper steps are required to increase the natural convection heat transfer by attaining higher Rayleigh numbers at the heat sink [10].

Phase changed materials (PCM): Phase changed materials is very popular now-a-days due to it's wide applications. It is already recognized as one of the most promising materials to store the excessive temperature in a form of latent heat [11]. Paraffin wax is one of the available materials which can be easily attached on the back side of the panel using turning pack as it has some low thermal conductivity. This material works very well in higher temperature condition as the wax starts melting properly. Cooling system using PCM decreases the operating temperature by almost 30°C with an overall power gain of 55% [12]. In addition to that, the reduction of temperature more than 30°C is also possible by adding fins on the back panel

instead of flat aluminum plate [13]. A typical schematic diagram of PV panel with PCM is shown in Figure 6 below:

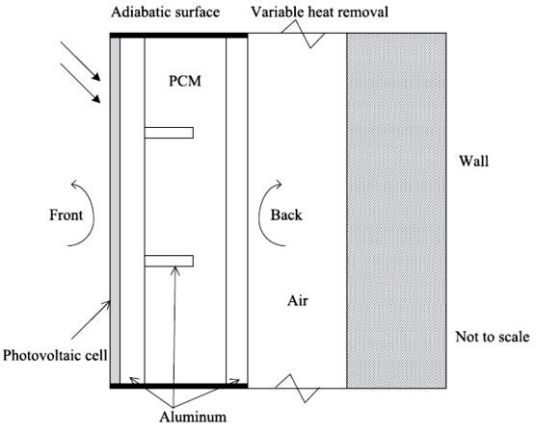

Figure 6. Schematic diagram of PCM based PV panel [14]

Cotton wick cooling: In this method, layer of wet cotton is attached on the back side of the panel which creates a moist environment. Usually this layer of cotton is connected with some water reservoir. It can decrease the temperature almost by 30% with a maximum efficiency of 10.2% while producing power [15].

Evaporative cooling technique: This cooling method is also promising as it does not suffer from any on site parasitic effect like other passive cooling technique. In real life we also have application of evaporative cooling where air motion is not desired. For example: recording studio, dark room for film development or places like hospital. Usually evaporation occurs when small portion of working fluid changes it's phase and withdraw the latent heat in a form of vapor. This system is developed which is made of copper and covered with synthetic clay to allow indirect evaporation. A clay layer with thickness of 2 mm performs best for evaporation process with maximum 19.1% enhancement in power generation [16].

Using dielectric medium: In this cooling method, the complete panel is immersed into the dielectric medium to reduce the heat. The solution could

be of any combination but the efficiency is not that much promising so far [17].

3 Analysis of different methods

It is of utmost importance to choose the right cooling technique while developing the hybrid thermal PV panel where the prime concern is to maximize the power generation by making the system as efficient as possible. To achieve the goal an appropriate cooling method must be selected from the vast options of active and passive techniques. The main goal is to choose a technique which is less expensive, eco-friendly and requires less operating cost. Here all the cooling techniques along with their possible limitations are described in Table 1:

Table 1. Analysis of different cooling methods

Cooling Type	Method Name	Main mechanism	Limitations
Active	Air flow based (PVT/AIR-REF)	Create a flat channel between solar cell and back wall for air flow	Not beneficial for area with very nominal air flow and channel depth should be minimum 10 cm in general
Active	Air flow based (PVT/AIR-TMS)	Create a channel with thin metal sheet in between cell and back wall	Metal shit must be placed in such way that there is enough spacing with the cell and back wall
Active	Air flow based (PVT/AIR-FIN)	Create a channel with multiple fins attached with back wall	Lack of proper attachment to the back wall could degrade the performance
Active	Fluid based (PVT/WATER-Nozzle)	Spraying water with nozzle by using motor	An array of nozzles required to ensure uniform distribution of temperature
Active	Fluid based (PVT/WATER-Trickling)	Dripping water from external sources throughout the front panel surface	Recycling the water for continuous usage.
Active	Fluid based (PVT/WATER-FGM)	A heat sink is created by adding graded materials	Required efficient design with proper use of graded material
Active	Refrigerant based	Refrigerant or coolant is pumped though a channel	It is very expensive and need to maintain different pressure levels throughout the system
Active	Heat pipe	Additional pipes are attached with the panel to pass the heat	Overheating of heat pipe may have an adverse effect
Passive	Submerged water cooling	Large amount of heat is dissipated by putting the panel into water	Leak proof design is mandatory to avoid liquid admission
Cooling Type	Method Name	Main mechanism	Limitations
Passive	Heat sink	Aluminum fins are attached on the back side of the panel to absorb the heat	Significant difference in temperature is required between the fins and ambient air to transfer the heat
Passive	Phase changed materials (PCM)	Materials like paraffin wax is used to store the latent heat	Works well only on high temperature condition due to it's higher melting point.

Passive	Cotton wick	Wet cotton is added on the rear side of the panel to create a moist condition due to capillary action	Highly depends on the wet capability of the cotton.
Passive	Evaporative	Latent heat is transferred via evaporation	Continuous supply of water required, under dry condition there could be crack on the clay.
Passive	Dielectric medium	This method involves immersing the front and back panel inside dimethyl-silicon oil	The percentage of temperature reduction is very nominal.

4 Result analysis and conclusion

Different techniques related with PV panel cooling have been discussed thoroughly. Each and every technique has some benefits along with some

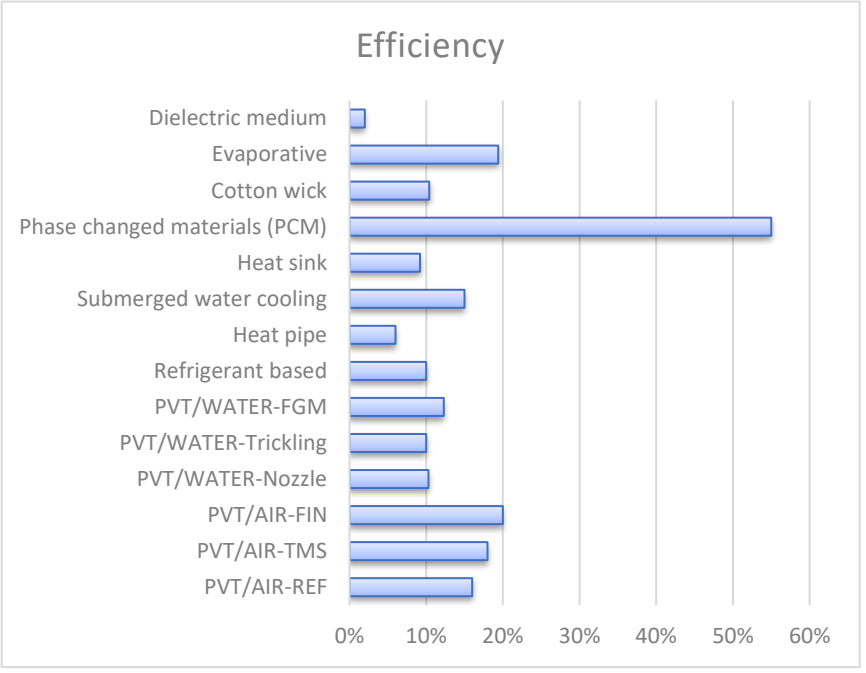

limitations. Here in the Figure. 7 a comparison based on efficiency is provided where the value ranges from 2-55%.

Figure 7. Comparison of efficiency for different cooling technique

In most cases active cooling and passive cooling techniques performs equally. But passive cooling technique is more preferred as it does not require external power to operate which also ensures the low operational cost of the system. Not only that passive cooling system is more eco-friendly as well. So

the applicable cooling technique solely depends on the application but passive cooling will be dominating on the coming days.

References

1. S. Nižetić, E. Giama, and A. M. Papadopoulos, "Comprehensive analysis and general economic-environmental evaluation of cooling techniques for photovoltaic panels, Part II: Active cooling techniques," Energy Convers. Manag., vol. 155, pp. 301–323, 2018.
2. K. Sopian, A. H. A. Alwaeli, A. N. Al-Shamani, and A. M. Elbreki, "Thermodynamic analysis of new concepts for enhancing cooling of PV panels for grid-connected PV systems," J. Therm. Anal. Calorim., vol. 136, no. 1, pp. 147–157, 2019.
3. J. K. Tonui and Y. Tripanagnostopoulos, "Improved PV/T solar collectors with heat extraction by forced or natural air circulation," Renew. Energy, vol. 32, no. 4, pp. 623–637, 2007.
4. H. G. Teo, P. S. Lee, and M. N. A. Hawlader, "An active cooling system for photovoltaic modules," Appl. Energy, vol. 90, no. 1, pp. 309–315, 2012.
5. B. Tashtoush and A. Al-Oqool, "Factorial analysis and experimental study of water-based cooling system effect on the performance of photovoltaic module," Int. J. Environ. Sci. Technol., vol. 16, no. 7, pp. 3645–3656, 2019.
6. M. Jaszczur, J. Teneta, Q. Hassan, E. Majewska, and R. Hanus, "An Experimental and Numerical Investigation of Photovoltaic Module Temperature Under Varying Environmental Conditions," Heat Transf. Eng., pp. 1–14, Dec. 2019.
7. F. Chen, F. Pao, and H. Yin, "14 - Advanced Building Integrated Photovoltaic/Thermal Technologies," T. M. Letcher and V. M. B. T.-A. C. G. to S. E. S. Fthenakis, Eds. Academic Press, 2018, pp. 299–319.
8. S. Vaishak and P. V Bhale, "Effect of dust deposition on performance characteristics of a refrigerant based photovoltaic/thermal system," Sustain. Energy Technol. Assessments, vol. 36, p. 100548, 2019.
9. G. M. Tina, M. Rosa-Clot, P. Rosa-Clot, and P. F. Scandura, "Optical and thermal behavior of submerged photovoltaic solar panel: SP2," Energy, vol. 39, no. 1, pp. 17–26, 2012.
10. U. J. Rajput and J. Yang, "Comparison of heat sink and water type PV/T collector for polycrystalline photovoltaic panel cooling," Renew. Energy, vol. 116, pp. 479–491, 2018.
11. H. Asgharian and E. Baniasadi, "A review on modeling and simulation of solar energy storage systems based on phase change materials," J. Energy Storage, vol. 21, no. July 2018, pp. 186–201, 2019.
12. S. Maiti, S. Banerjee, K. Vyas, P. Patel, and P. K. Ghosh, "Self regulation of photovoltaic module temperature in V-trough using a metal–wax composite phase change matrix," Sol. Energy, vol. 85, no. 9, pp. 1805–1816, 2011.
13. J.-J. Huang and D. Shiung, "The signaling efficiency of group mobility management in Cellular IP," J. Chinese Inst. Eng., vol. 34, no. 7, pp. 957–966, Oct. 2011.
14. T. Ma, H. Yang, Y. Zhang, L. Lu, and X. Wang, "Using phase change materials in photovoltaic systems for thermal regulation and electrical efficiency improvement: A review and outlook," Renew. Sustain. Energy Rev., vol. 43, pp. 1273–1284, 2015.

15. M. Chandrasekar, S. Suresh, T. Senthilkumar, and M. Ganesh Karthikeyan, “Passive cooling of standalone flat PV module with cotton wick structures,” Energy Convers. Manag., vol. 71, pp. 43–50, 2013.
16. A. H. Alami, “Effects of evaporative cooling on efficiency of photovoltaic modules,” Energy Convers. Manag., vol. 77, pp. 668–679, 2014.
17. L. Liu, L. Zhu, Y. Wang, Q. Huang, Y. Sun, and Z. Yin, “Heat dissipation performance of silicon solar cells by direct dielectric liquid immersion under intensified illuminations,” Sol. Energy, vol. 85, no. 5, pp. 922–930, 2011.

THREE-DIMENSIONAL CRUSTAL IMAGE OF ARRAIOLOS AFTERSHOCK SEQUENCE, EARTHQUAKE OF M=4.9, IN CENTRAL PORTUGAL

INES HAMAK

Institute of Earth Science (IIFA), University of Evora, Rua Romão Ramalho, 59. 7000-671, Évora, Portugal, hamak.ines@gmail.com

JOSÉ BORGES, MOURAD BEZZEGHOUD

Department of Physics (ECT), Institute of Earth Science (IIFA), University of Evora, Rua Romão Ramalho, 59. 7000-671, Évora, jborges@uevora.pt, mourad@uevora.pt

PIEDADE WASHILALA

Instituto Superior de Ciências de Educação da Huíla, Departamento de Ciências da Natureza, Angola, piedadewachilala@gmail.com

This study presents preliminary results of the 3D model of P and S velocity anomalies and Vp/Vs ratio distribution. This work is based on a 4.9 ML magnitude earthquake which occurred on January 15th, 2018 at 11:51 UTC in *Aldeia da Serra* in the Northeast of Arraiolos (Portugal). The hypocentral location, determined by the Instituto Português do Mar e da Atmosfera (IPMA), has coordinates 38.79 N, 7.93 W at 11 km depth. A sequence of 317 local events were inverted in order to obtain velocity contrast in all directions and relocate accurately these aftershocks. The computation of the inversion was performed using LOTOS code *(Ivan Koulakov, 2009)* which has the ability to make a simultaneous inversion for the source parameters and velocity model using several parameterization grids. In order to evaluate the limitation of model resolution, synthetic tests were performed using checkerboard method. Several models have been tested to make this resolution analysis. Despite the difficulty to find correlation between seismicity and faults in the region, the interpretations led to geological assumptions that relate P and S anomalies to tectonic features.

1. Introduction

An earthquake occurred on the 15th of January 2018 in Arraiolos, a region that is located in the north of Évora (Portugal). This earthquake was the biggest in the area since 1969 with a ML=4.9 located in a depth of 11km. This event has generated several questions about the tectonic of the region.

Therefore, some geological and seismological studies have been conducted in the region *(Wachilala et al (2019), Araújo et al (2018), Matos, et al (2018), Matias, et al (2019))*, showing a moderate seismicity linked to the slow plate movement of Iberia. Naturally, this low seismicity generates a lack of correlation between earthquake distribution and geological faults. Even if some faults have been mapped, none of them are linked to the seismicity of the studied region. That makes seismological interpretations hard to develop.

The seismic sequence after the main shock, was monitored by named Arraiolos temporary seismic network (ATSN), composed of 14 broadband stations (CMG 6TD, 30s) of the Institute of Earth Sciences (ICT, Évora) and 21 short-period stations (CDJ, 2.0 Hz) of the Instituto Dom Luiz (IDL, Lisbon). This seismological array has recorded 317 events mainly distributed in *Aldeia da Serra* region. Moreover, earthquakes locations are accurate, due to

the fine station azimuthal coverage (*Borges, et al., 2018))* which led to a correct picking of arrival times that will, indeed, minimize inversion errors.

Due to the complexity of the seismicity observed in Arraiolos, a tomographic study was conducted to better understand these tectonic phenomena. Thus, by using LOTOS code, produced by Ivan Koulakov (2009), performing travel time inversion, a velocity distribution in 3 directions will be obtained. After obtaining the crustal velocity model we will be able to target the geological layer which is responsible for this complex deformation. Also, seismogenic zone will be detected and related to focal mechanisms obtained for this aftershock concentration.

2. Geological context

Arraiolos is a part of Ossa Morena Zone (OMZ) where an important presence of variscan orogeny structures that characterize the tectonic of a big part of Portugal can be observed Figure 1.B. However, on the geological map of the studied area, aftershock concentration is mainly localized in tectonic structures that come from Cambrian Variscan orogeny (Figure 2). Moreover, the rocks that compose this region have volcanic, plutonic, sedimentary and metamorphic origins and the volcanism that is related to the studied region is coming from Palaeozoic period according to *Custodio et al. (2015)*, study.

Additionally, neotectonics studies made in the region, mapped some active faults which are Lower Tagus Valley, Ponte de Sor, Serra da Ossa, Ciborro, Messejana, Vidigueira-Moura, Torrao, Grandola and the Santa Susana faults. Nevertheless, those faults are not responsible for the seismicity in the region and because of the low deformation it is difficult to detect outcropping faults. The difficulty to find a correspondence between mapped faults and seismicity distribution complicates the seismological and tectonic interpretations.

A geological study made by *Araujo et al. (2010).*, has showed lineaments of active faults in the region. Therefore, the authors built a model which showed the presence of Ciborro and São Gregorio faults, characterized by a dextral strike-slip focal mechanism oriented WNW-ESE, that intersect in *Aldeia da Serra*, highest point of the region, which describe a reverse focal mechanism that was qualified as a “push-up”. Indeed, this geological model proposed by *Araujo et al. (2010)* is a hypothetical model that must be explored.

A.

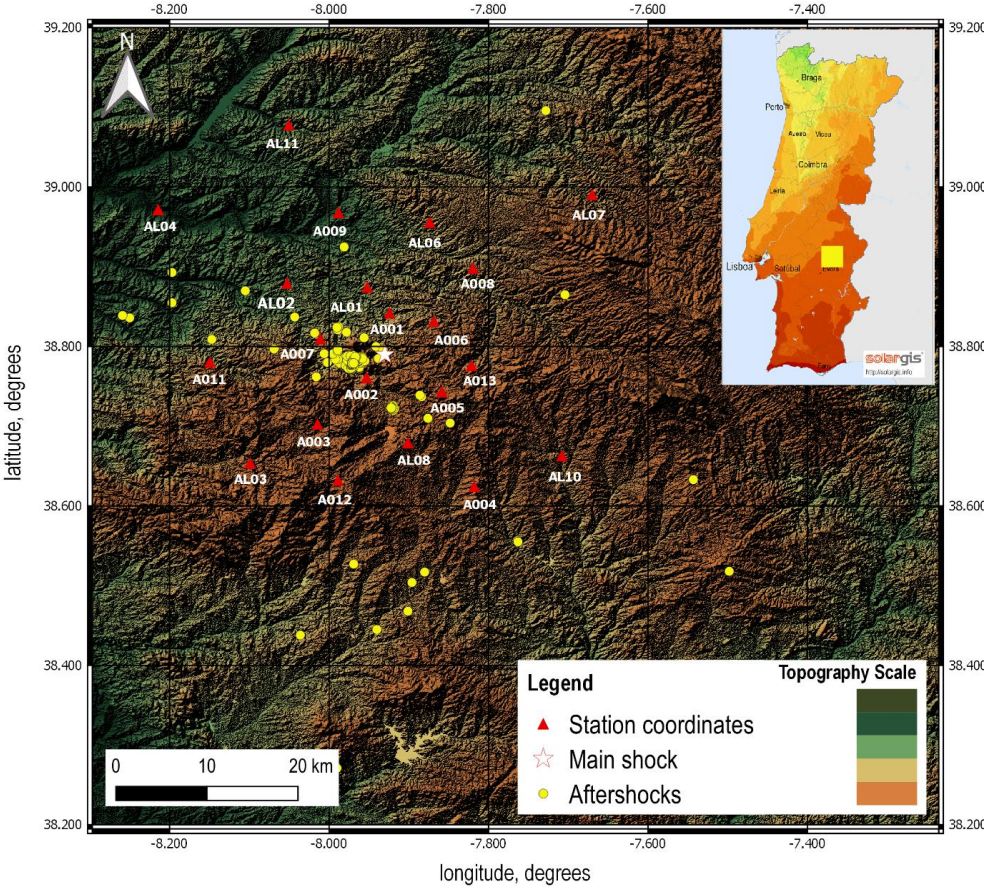
-8.200
-8.000
-7.800
-7.600
-7.400
39.200
39.000
38.800
38.600
38.400
38.200
latitude, degrees
longitude, degrees
N
AL11
AL04
A009
AL06
AL07
A008
AL02
AL01
A001
A006
A007
A011
A013
A002
A005
A003
AL08
AL10
AL03
A012
A004
0
10
20 km
Legend
Station coordinates
Main shock
Aftershocks
Topography Scale
Braga
Porto
Aveiro
Viseu
Coimbra
Leiria
Lisboa
Setúbal
Évora
solargis

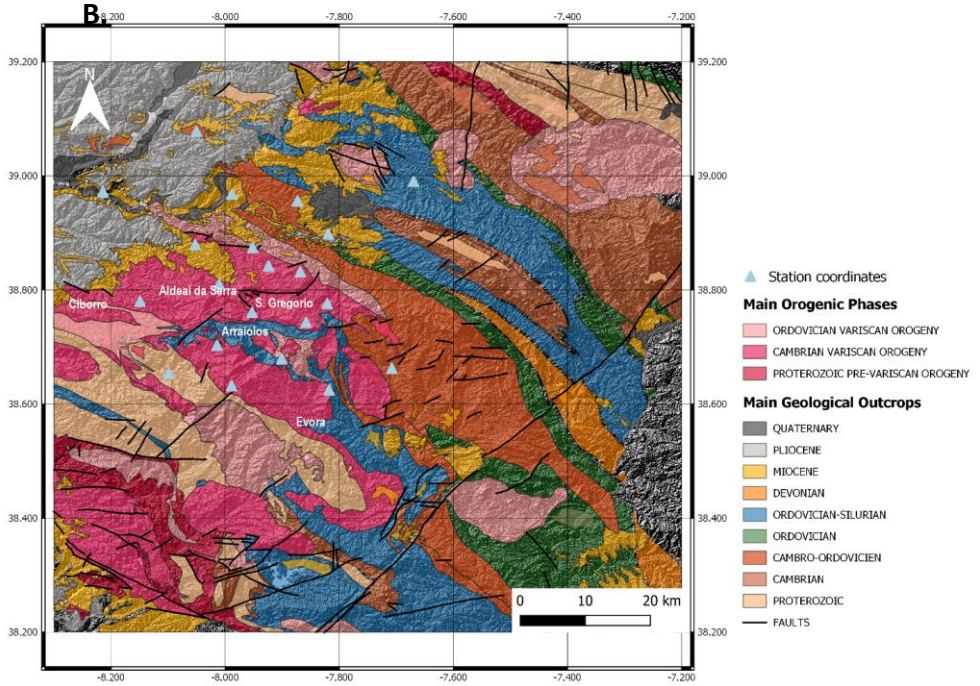

Figure 1. Seismological network and aftershock distribution within topographic and geological map of Arraiolos region. **A.** Topographic map describing the spatial distribution, within the studied area, of the 21 short period stations (CDJ, 2.0 Hz) of the IDL (Instituto Dom Luiz) represented in *red triangles* and the 317 aftershocks which are represented in *yellow dots*. The *white star* indicates the main shock located by Instituto Português do Mar e da Atmosfera (IPMA) **B.** Geological map which shows the main structural elements of Arraiolos and Evora regions. *Blue triangles* represent the seismological stations that have recorded the aftershock sequence.

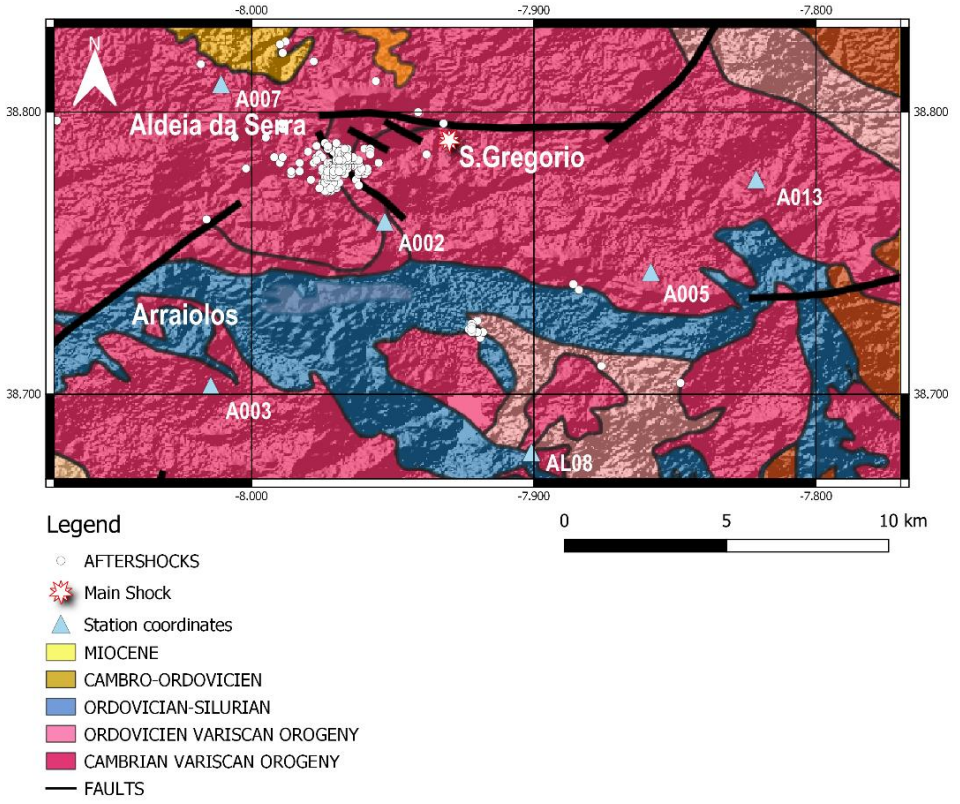

Figure 2. Well covered area in terms of ray density selected by the inversion software LOTOS. *Yellow dots* represent 6 temporary seismological stations which appear in the region and white dots represent aftershock spatial distribution and the *white star* refers to the main shock location. This geological map zoom will be the support for relating tectonic features to velocity anomalies.

3. Data selection

A number of 317 aftershocks, of a magnitude lower than 4.0, to perform tomographic inversion recorded by 21 short-period stations (CDJ, 2.0 Hz) of the IDL, was selected (Figure 1). For the visualization vertical and horizontal cross sections, crossing the aftershock area, were chosen (Figure 3). 4235 P (47.08%) and 4761 S (52.92%) arrival times have been recorded. Moreover, most of events are recorded by more than 10 stations; only 5 events are recorded by a lower number of stations. Also, aftershocks are concentrated in a local region in a depth which goes from 10km to 12km (Figure 3).

Furthermore, the starting 1D velocity model used in this inversion is showed in Table 1. This model is the same which was used for aftershocks location. It contains P velocity values and a Vp/Vs ratio of 1.7. From the moment when the inversion is performed, S velocities are going to be calculated from Vp/Vs ratio and P velocities distributed in the 6 different homogeneous velocity layers (Table 1).

Table 1: 1D starting velocity model for real data inversion. Vp/Vs ratio is about 1.7.

DEPTH (km)	P VELOCITY (km/s)
0	5.8
3	5.95
6	6.1
9	6.2
12	6.3
15	6.4

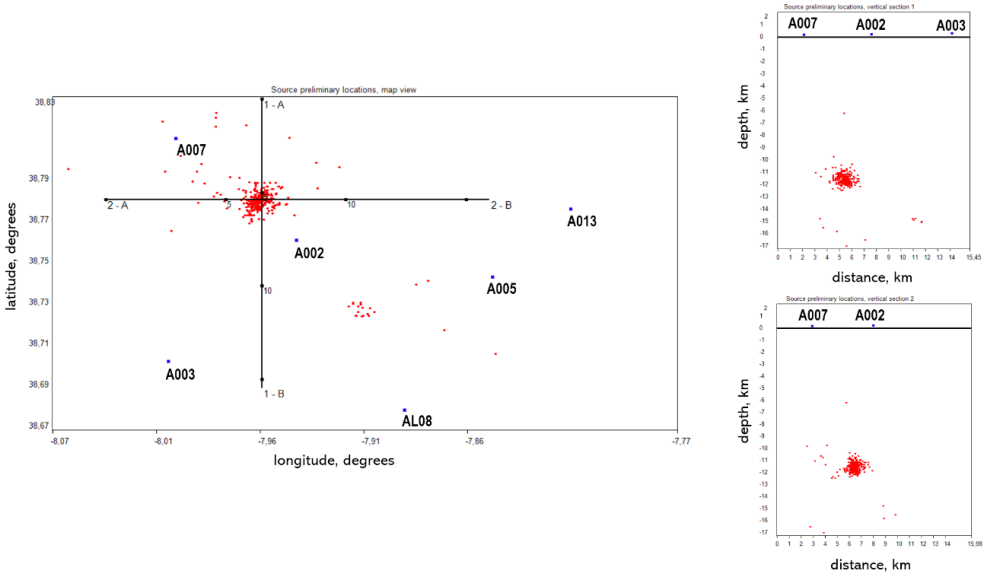

Figure 3. A- Preliminary location of the 317 aftershocks, which appears in *red dots*, carried out by LOTOS code on the first step after 1D velocity model optimization. *Blue squares* indicate the 6 temporary stations appearing in the selected area. B- Visualization of sources spatial distribution within depth beneath horizontal and vertical sections, respectively 2A-2B and 1A-1B.

4. Inversion methodology

To provide more information about Arraiolos seismicity and its deformation characteristics, a seismic tomography was carried out using LOTOS software *(Ivan Koulakov, (2009))*. In fact, the program is based on an iterative method which performed a simultaneous inversion of the source locations and 3D velocity model. In order to obtain a tomographic image of the studied region, two important input data are required. They are the following ones:

- Sources coordinates
- P and S waves arrival times

In addition to those data, a parameterization of the area must be done. The parameters which must be fixed are the following ones:

- 1D velocity model (initial model) (Table 1).
- Grid parameters (nodes, cells, grid spacing, grid orientation)
- Calculation parameters (inversion, matrix computation, source location)

Indeed, this iterative method can provide, on each iteration, an improved 3D velocity model which allows the sources location to be as accurate as possible.

The added value of this method is related to the fact that the 1D velocity model is optimized before inversion begins and to the coupled inversion of sources location and 3D velocity model as well. Moreover, the ray tracing method is based on a 3D bending algorithm which stability has been verified by disturbing the travel times in a synthetic model.

In our study, LOTOS software *(Ivan Koulakov, (2009))* is used to obtain a three-dimensional image of the Arraiolos region in terms of velocity distribution. It is noted that the code will select the area of a maximum ray coverage (Figure 3). For the inversion, we have selected 317 events which was well located by 21 deployed stations and 4235 P and 4761 S waves arrival times recorded. At the end of the inversion, the difference between observed and calculated travel times are related to picking, location and starting velocity model errors. That is why we must know all the details about the location and arrival times picking to be able to make consistent interpretation of velocity anomalies distribution.

After starting the inversion, the first step performed is the optimization of the initial 1D velocity model and the preliminary sources location (Figure 3). On the first iteration, grid construction parameters are fixed and the sources location within the 3D velocity model can begin and know an improvement iteration by iteration. Thus, travel times calculation using bending method is performed to allow the matrix calculation which is going to be inverted in order to provide P and S waves velocity distribution all along the area. Moreover, concerning grid parameters, nodes distribution is going to be done in function of ray density. The minimal nodes spacing refers to the area of an important ray coverage.

5. Synthetic Tests

We performed synthetic tests to evaluate the resolution limits of our dataset and the smearing effect in both vertical and horizontal directions. We have processed several checkerboard models to see which of them gives significant results. The inversion was run by following the same workflow and inversion parameters used for the real model. Moreover, synthetic travel times are computed by using bending ray tracing method *(Ivan Koulakov, (2009))* for all the actual source-receiver pairs.

The inversion starts by building several checkerboard models. The principle is based on assigning, as an arbitrary model, P and S exaggerated anomaly amplitude in a typical 3D checkerboard grid pattern. At the end, the inversion quality is evaluated by analysing the similarity between the final model and the arbitrary one. If both are close enough, we can say that the area resolution is robust.

In our case, we created 4 models with anomaly dimension of 4km in X and Y directions with an empty space of 2.5km and 3km. We performed synthetic model inversion for both ±7% and ±12% P and S anomalies amplitude. For the last model we adjusted P and S weight. The resolution and the recorded number of S waves are higher than the P waves. Thus, we have fixed a weight of 0.7 and 1, respectively, for P and S velocity models.

The results show that the horizontal reconstruction is well resolved for areas which correspond to a good ray coverage (Figure 5). We can notice as well, that the patterns are well resolved for S waves in all models. The best-fit correspond to the last model where a lower weight value for P velocity model was assigned (Figure 4, D). After adjusting the weight value, anomalies are less smeared and patterns are robustly resolved both, for P and S waves.

Moreover, inversion is unable to resolve velocity anomalies that have dimensions which are different than 4km.

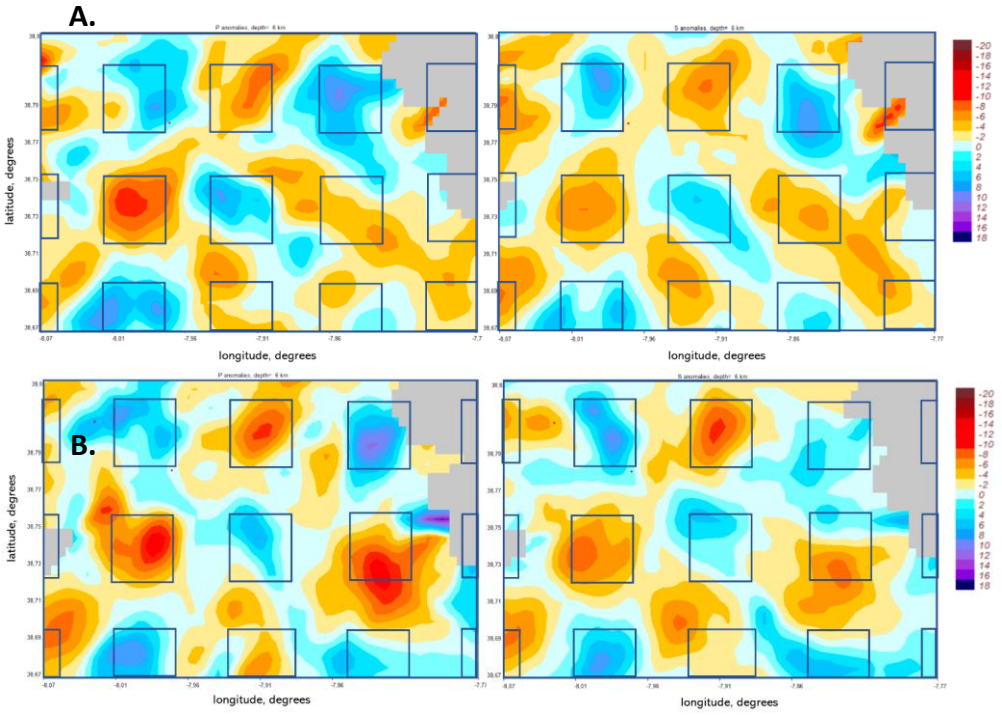

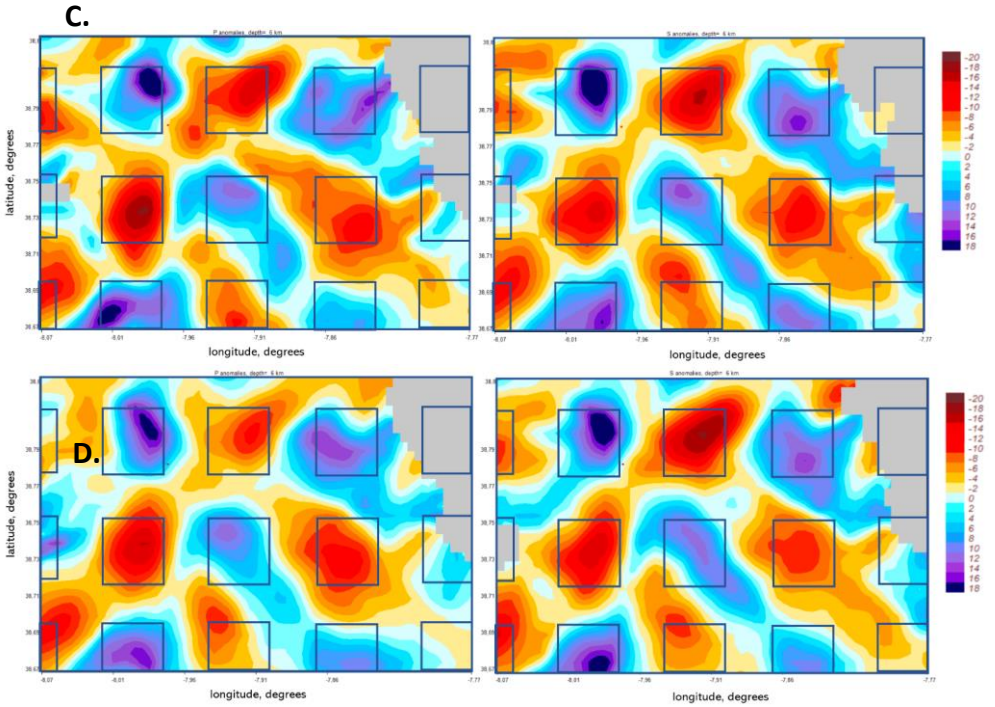

Figure 4. Those figures represent 4 models of horizontal synthetic inversion results to identify the model resolution limits in a depth of 4km. A- Model 1 has as parameters respectively 4km,4km,2.5km, ±7% for x, y, empty space dimensions and P and S amplitude anomalies. B- Model 2 has as parameters respectively 4km, 4km, 3km, ±7% for x, y, empty space dimensions and P and S amplitude anomalies. C- Model 3 has as parameters respectively 4km, 4km, 2.5km, ±12% for x, y, empty space dimensions and P and S amplitude anomalies. D- Model 4 has as parameters respectively 4km, 4km, 2.5km, ±12%, 0.7, 1 for x, y, empty space dimensions, P and S amplitude anomalies and weights for P and S velocity model. *Blue squares* are indicating the configuration of anomalies.

To see which model corresponds to the best checkerboard reconstruction, the reduction variance of P and S waves is a support (Table 2). By analysing the table 2, it appears that the best model reconstruction is the third and fourth ones as we can see in Figure 4, C & D.

On the other hand, vertical resolution is poorer than in the horizontal directions, because of the trade-off between velocity model and sources parameters. Patterns are well resolved for most of the models. However, anomalies smearing is clearly observed especially for Model 1 and 2 (Figure 4). Also, the corner of the area is characterized by a bad resolution and patterns which are badly resolved. It shows that we can robustly resolve the inversion in the area where most of earthquakes are located (Figure 3 & 5).

By making those synthetic tests using checkerboard method, we can know which area should be considered for the interpretation of real data inversion.

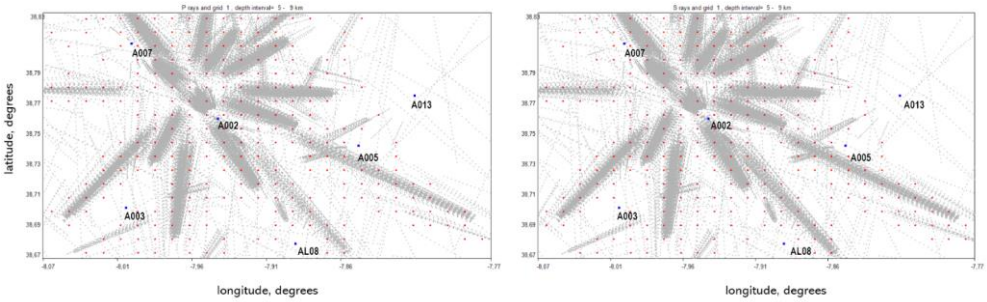

Figure 5. Example of ray spatial distribution for P and S waves from 317 events. *Blue squares* represent seismological stations and *grey dots* indicate the ray paths in a depth interval of 5-9km. *Red dots* indicate node parametrization in the area of study which is distributed in function of ray density.

Table 2: Synthetic model's parameters and variance reduction of the last iteration.

Models	Anomaly values (%)	ΔX (km)	ΔY (km)	ΔZ (km)	Empty space (km)	P weight	S weight	P Varian reduction
1	7	4	4	20	2,5	1	1	28.5644
2	7	4	4	20	3	1	1	27.5578
3	12	4	4	20	2,5	1	1	45.5346
4	12	4	4	20	2,5	0,7	1	42.7484

6. Inversion results

After performing real data inversion, we obtained a distribution of P and S velocity anomalies within all directions. Moreover, iteration by iteration the 3D model is improved simultaneously with sources locations that led us to make assumptions about the potential seismogenic zone and its related tectonic units.

First, we can observe anti-correlation between P and S anomalies, with positive P anomalies and negative S anomalies (Figure 6, A & B). Not a high negative contrast for P waves. Moreover, a big Vp/Vs contrast is observed in the area of aftershocks concentration (Figure 6, C).

These two observations suggest either the presence of fluids or volcanoes (this assumption have to be confirmed with previous studies). Residuals obtained at the end of the inversion have satisfying values. It represents 70.23 % for P and 70.80 % for S waves reduction variance. Moreover, events location has a precision of 0.021s for P waves and 0.032s for S waves.

The anti-correlation of P and S anomalies, located in the area of concentrated aftershocks, leads to a high Vp/Vs contrast which suggest the presence of a fluid or a material with specific properties. Moreover, it is obvious that a good resolution will be observed in area of high ray density which correspond to a depth that goes from 5km to 9km Figure 5**.** Areas on the corner of the region are not well resolved by the inversion because of the poor ray coverage, as we

have seen on synthetic tests results. Therefore, inversion interpretation will not be consistent in area edges.

Furthermore, these anomalies correspond to Variscan orogeny in terms of tectonic context. Thus, positive anomalies correspond to Ordovician Variscan orogeny and negative anomalies to Cambrian variscan orogeny (Figure 2). On both cross sections, an important positive anomaly is observed linked to Ordovician variscan orogeny. This anomaly is very well correlated with the seismogenic zone where we can observe an agglomeration of aftershocks. Nevertheless, the aftershock distribution is not describing a specific trend. We cannot identify or correlate event concentration to an existing fault. This shows probably the complexity of the active tectonics in this region.

Matos and al. 2018, study have provided some assumptions regarding Arraiolos seismic zone which was divided in two parts, the South and the North which describe different seismicity. One of the hypotheses was related to thermal structure and thus rheological differences which suggest a vertical magmatic flow in WOMZ region that thermally weakens the lower crust and generates stress concentration in the middle and upper crust.

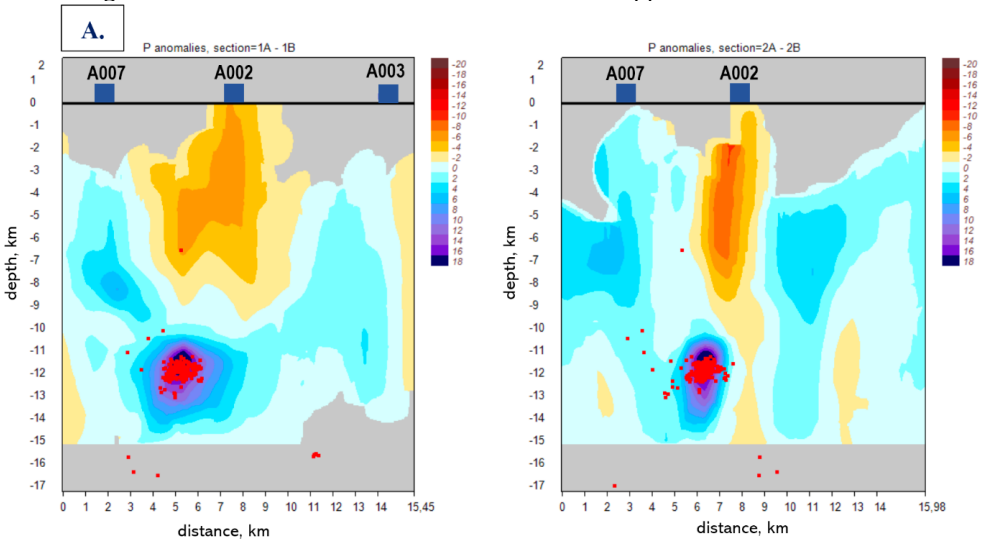

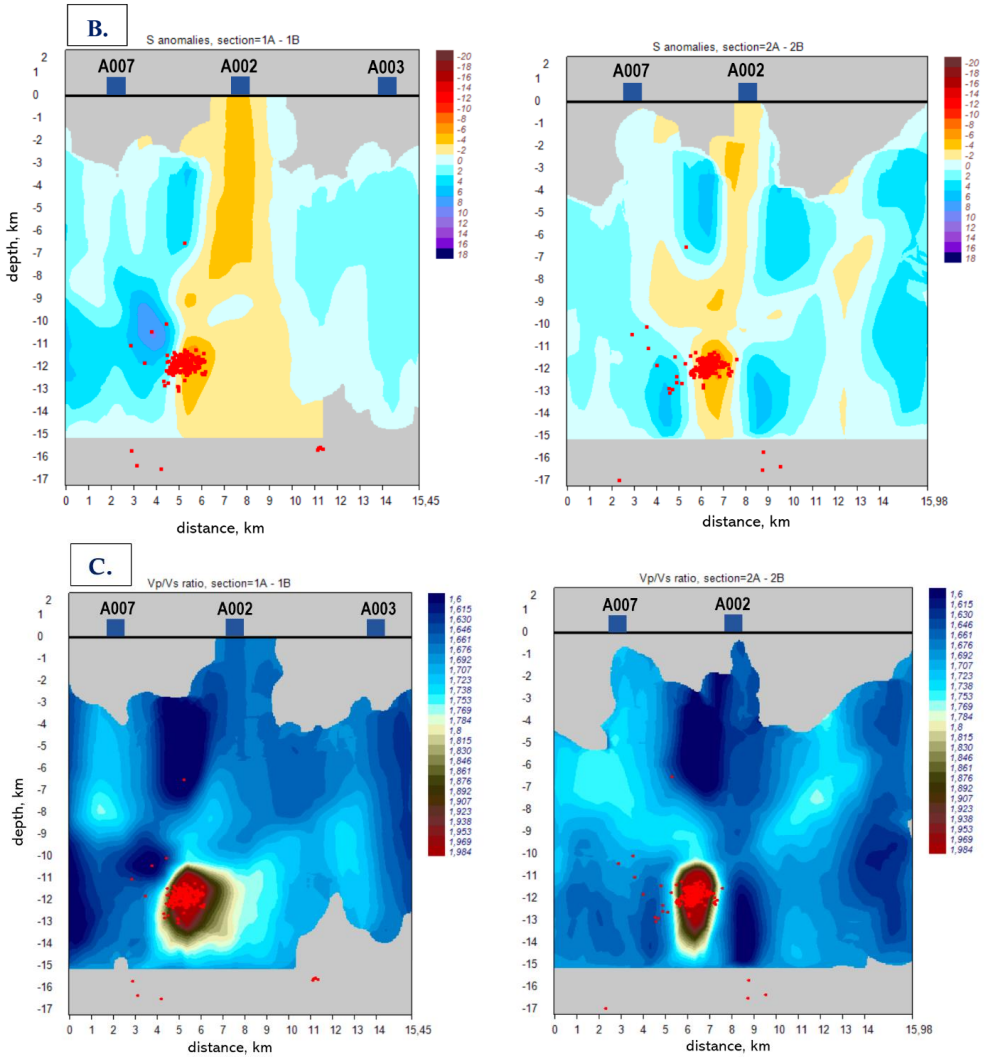

Figure 6. Real data inversion results. A- P anomaly distribution beneath the two cross section 1A-1B and 2A-2B. B- S anomaly distribution beneath the two cross section 1A-1B and 2A-2B. C- Vp/Vs distribution beneath the two cross section 1A-1B and 2A-2B. *Blue squares* represent seismological stations and *red dots* indicate aftershocks locations.

7. Discussion and conclusion

This tomographic study was performed for the first time in Arraiolos, in order to find geological features which could be responsible for the seismicity of the region. Also, it allows us to relocate sources within depth that knows an improvement simultaneously with the 3D velocity variations. Nevertheless, a poor ray coverage due to the distribution of earthquakes in one point in *Aldeia da Serra*, was noted. The inversion was unable to cover the entire area of interest, and therefore a poor resolution was clearly observed. Inversion results have

provided information leading to some assumptions, however data that we have are not sufficient to generate more explanations about Arraiolos seismicity causes. Hence, more data must be added to this study in order to have a better coverage of the area in terms of ray distribution that will allows us to make more consistent interpretations. Data that we need to introduce, besides local events, are teleseismic events recorded by the same temporary station network as used for the 317 aftershocks recordings. In addition to this temporary station network, we thought about considering the Instituto Português do Mar e da Atmosfera IPMA and DOCTAR networks which will bring supplementary records, but also the ICT broadband temporary stations unused in this first stage of study.

References

1. Araújo, A., Caldeira, B., Martins, A., Borges, J,F., Araújo, J., Moreira, N., Maia, M., Vicente, S., Afonso, P., Espanhol, D., Bezzeghoud, M. (2018). Macrossismicity associated with the Arraiolosearthquake of January 15, 2018with M = 4.9 and possible implications in the geometry of the rupture. *Revista Portuguesa de Vulcanologia.*
2. Araújo, A., Matos, C., Martins, A. (2010). A elevação de Aldeia da Serra (Arraiolos): um "push up" activo associado à falha de Ciborro e ao lineamento de S. Gregório? *GEOTIC – Sociedade Geológica de Portugal **VIII** Congresso Nacional de Geologia*
3. Bellalem, F., Bounif, M. A., & Koulakov, I. (2015). P and S waves tomographic analysis of the area of El Asnam's 1980 ms 7.3 earthquake (Algeria) from its aftershock sequence. *Journal of Seismology*, ***19*(1)**, 253–264. https://doi.org/10.1007/s10950-014-9464-x
4. Custódio, S., Dias, N. A., Carrilho, F., Góngora, E., Rio, I., Marreiros, C., Morais, I., Alves, P., & Matias, L. (2015). Earthquakes in western Iberia: Improving the understanding of lithospheric deformation in a slowly deforming region. *Geophysical Journal International*, ***203*(1)**, 127–145. https://doi.org/10.1093/gji/ggv285
5. Koulakov, I. (n.d.). *Local earthquake tomography (LET) scheme LOTOS code (version 12) Brief description of workflow Structure of the LOTOS code : Root folder : version **12,** **25***.
6. Koulakov, I. (2009). LOTOS code for local earthquake tomographic inversion: Benchmarks for testing tomographic algorithms. *Bulletin of the Seismological Society of America*, ***99*(1)**, 194–214. https://doi.org/10.1785/0120080013
7. Koulakov, I. (2012). *Code LOTOS-12 for 3D tomographic inversion based on passive seismic data from local and regional events Table of content :* 1–59.
8. Koulakov. I, et al. (2007). P and S velocity structure of the crust and the upper mantle beneath central Java from local tomography inversion, *JOURNAL OF GEOPHYSICAL RESEARCH, VOL. **112**, B08310, doi:10.1029/2006JB004712, 2007.*
9. Lévěque, J. -J, Rivera, L., & Wittlinger, G. (1993). On the use of the checker-board test to assess the resolution of tomographic inversions. *Geophysical Journal International*, ***115*(1)**, 313–318. https://doi.org/10.1111/j.1365-246X.1993.tb05605.x
10. Matias L., Rio, I., Waschilala, P., Vales, D., Borges, J.F., Dias, N., Carrilho, F., Caldeira, B., Custodio, S., Fontiela, J., Bezzeghoud, M., Araujo, A., Corela, C. (2019). The seismic sequence of Arraiolos, Portugal, in January 2018. *EGU General Assembly 2019.*
11. Matos, C., Custódio, S., Batló, J., Zahradník, J., Arroucau, P., Silveira, G., & Heimann, S. (2018). An Active Seismic Zone in Intraplate West Iberia Inferred From High-

Resolution Geophysical Data. *Journal of Geophysical Research: Solid Earth*, *123*(4), 2885–2907. https://doi.org/10.1002/2017JB015114

12. Veludo, I., Dias, N. A., Fonseca, P. E., Matias, L., Carrilho, F., Haberland, C., & Villaseñor, A. (2017). Crustal seismic structure beneath Portugal and southern Galicia (Western Iberia) and the role of Variscan inheritance. *Tectonophysics*, ***717,*** 645–664. https://doi.org/10.1016/j.tecto.2017.08.018
13. Wachilala, P., Borges, J.F., Matias, L., Rio, I., Fontiela, J., Oliveira, R., Caldeira, B., Bezzeghoud, M., Araújo, A., Custódio, S., Vales, D., Carrilho, F., Dias, N. (2019). Análise da distribuiçãoespaço-temporal da sismicidade na zona de arraiolosnoperíodo de janeiro - maio de 2018.*APMG 2019.*

A STUDY ON THE GYROSTAT SATELLITE

JEBUN NAHER SIKTA
Dept. of Physics, Earth and Space Science, University of Evora, Portugal.
Email: jebunphy@gmail.com

The focus of this study is on theoretical observations of the rotational motion of a gyrostat satellite moving along a circular orbit in the central Newtonian force field. Distinction between the circular and eliptical orbits is mentioned. Scope of work in studying gyrostat satellite in elliptical orbits is reported.

1. Introduction

One of the main attention of astrophysists is the study of the motion of celestial objects of our solar system. It is interesting to study the planetary theories and the motion of the artificial satellites around the Earth. Gravitational torques for attitude stabilization has the advangate that it allows the desired attitude to be mantained for an infinite periode of time in the absence of certain disturbance. However, it has certain disadvantages as well. There are little choices in the attitude that satellite maintain. It becomes difficult to maintain the desired attitude within a small tolerance. The behavior of such satellites can be altered significantly with the incorporation of a spinning rotor in it`s design. Longman in 1971 described the behavier of the special class of gyrostat configarations where the internal angular momentum vector of rotor axis is lying in any plane formed by two principle axises of the satellite [2]. Surchev in 2001 gave an analytical solution to the problem of determining all equilibria of a gyrosta satellite in a circular orbit when internal angular momentum of the gyrostat satellite is collinear to its principal axis of inertia [3].

In this paper, we have repored the progresses that have been made during the last few decades in the study of gyrostat satellite that is moving along a circular orbit in central Newtonian gravitational field. Recommendations for future work in elliptical orbits are reported.

2. Kinetic energy equations

Let us consider the attitude motion of a gyrostat satellite with statically and dynamically balanced rotors inside. The angular velocities of rotors are constant with respect to the satellite. The center of mass (O) of gyrostat satellite is located in a circular orbit. We consider two Cartesian coordinate systems i.e., orbital coordinate system (OXYZ) and gyrostat-fixed coordinate system (OX"'Y"'Z"'). Both of the systems origin at the center of mass (O) of the gyrostat satellite. OZ axis, of the orbital coordinate system (OXYZ), directes along the radius vector connecting the centers of mass of the Earth and the gyrostat satellite. OX axis directs along the vector of linear velocity of the center of mass (O). OX"'Y"'Z" system; OX"', OY"', OZ"' are the principal central axes of inertia of the gyrostat satellite. The orientation of the OX"'Y"'Z"' coordinate system with respect to the OXYZ system is defined by Euler angles; ϕ, θ and $\emptyset$

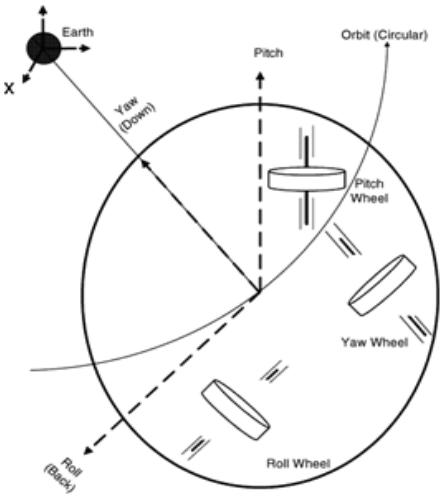

Figure 1: System representation[1]

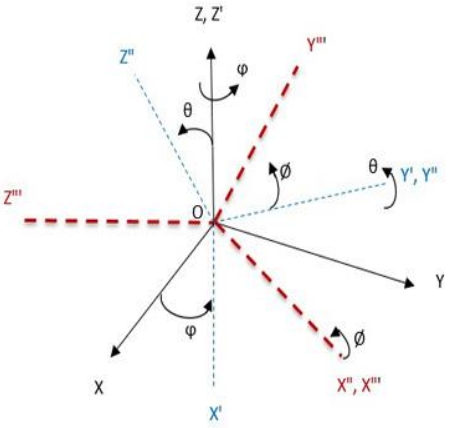

Figure 2: Euler angles

Then the kinetic energy of a gyrostat satellite is given as [4],

$$T = \frac{1}{2}(\mathrm{Ap}^2 + \mathrm{Bq}^2 + \mathrm{Cr}^2) + \bar{h_1}p + \bar{h_2}q + \bar{h_3}r$$

Where $\bar{h_1}, \bar{h_2}, and\ \bar{h_3}$ are the projection of gyrostat momentum vector on OX"', OY"', OZ"' axises. A, B, C are the principal central moment of inertia of a given general shapes. *p*, *q,* and r are the projections of the angular velocities on three axies of OX"'Y"'Z"' coordinate system.

3. Circular and Elliptical Orbits

When people first discovered that planets orbited around the sun, they thought that the orbits would be in the shape of a circle. In 1601, Johannes Kepler determined that the planets actually orbit in *ellipses* around the sun. An ellipse looks like a circle that has been "squashed" slightly, like an oval, or like an egg. Kepler also found that when a satellite orbits in an ellipse, it moves faster when it is close to the object that it is orbiting and slower when it goes farther away. Eccentricity is a measure of how circular a satellite's orbit is. For a perfectly circular orbit, the eccentricity is zero; elliptical orbits have eccentricities between zero and one.

4. Recommendation of future work

Until date, dynamics of rotational motions of gyrostat satellite in circular orbit have been studied for a particular ($h1 = 0, h2 \neq 0, h3 = 0$) and the general ($h1 \neq 0, h2 \neq 0, h3 \neq 0$) cases. Dynamics of rotational motion relative to centre of mass in elliptical orbit could be invastigated in near future. In studying such dynamics, it is recommended to start with special/particular case to avoaid complexicity. After studying spacial case, one can proceed for general case.

References

[1] L.F.F.M. Santos, "Gyrostat dynamics on a circular orbit". PhD Thesis, Universidade de Beira Interior, Portugal (2015).

[2] R. W. Longman, "Gravity gradient stabilization of gyrostat satellites with rotor axes in principal planes," Celest. Mech. **3** (2), 169–188 (1971).

[3] V. A. Sarychev and S. A. Mirer, "Relative equilibria of a gyrostat satellite with internal angular momentum along a principal axis," Acta Astronaut. **49** (11), 641–644 (2001).

[4] V.A. Sarychev, S.A. Gutnik, Relative Equilibria of a Gyrostat satellite, Cosmic Research, **22**(3), pp.257-260, 1984

THE EVOLUTION OF NOVEL ASEISMIC STRUCTURE DESIGN: METAMATERIALS

YUFAN DING
Ciências da Terra e do Espaço, Universidade de Evora, Evora, Portugal,
Scienza e Tecnologia dei Materiali, Politecnico di Torino, Turin, Italy
yding@uevora.pt

This article is a review of aseismic metamaterials. Metamaterials is an emerging achievement that has already been successfully applied in the field of electromagnetic wave. The periodic structure of metamaterials has the function of modulating wave propagation. Thus, considerable attention is drawn for its potential application in earthquake resistance. In this article, based on up-to-date studies, different designing concepts and some in-situ experiment have been introduced, the corresponding mechanism are explained as well.

5 Introduction

1.1. *Background of Metamaterials*

In late 1960s, the former Soviet scientist V. G. Veselago 1 had come up with the concept of a substance with negative permeability and permittivity, through deduction he has predicted the unusual electrodynamic properties of this material, such as negative refraction index, opposite direction of phase velocity and group velocity. Such material can hardly be found in nature, but it is possible to obtain equivalent properties by artificial tailored periodic structures (Figure 1.), which was proved by D. R. Smith et al via direct calculation 2. One year later, R. A. Shelby et al made the experimental verification, that a structed metamaterial (Figure 2.) exhibits a negative refraction index 3. Till nowadays, metamaterials have been extensively researched and some applications have already been carried out leady wave antenna, infrared stealth, and photonic crystals.

Due to the mathematical analogy of acoustic wave and electromagnetic wave, their problems can be solved with same methodology 5. Scientists have been searching the way to control elastic waves, leading to the application in seismology and civil engineering.

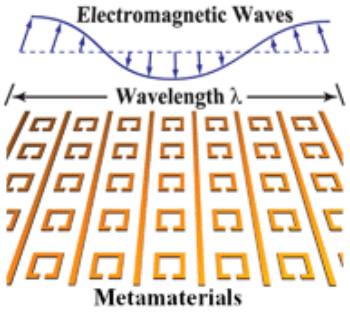

Figure 1. Periodic structures with unit distance much smaller than wavelength 4.

Figure 2. The left-hand metamaterial sample which consists of square copper split ring resonators and copper wire strips on fiber glass circuit board material.

1.2. *Seismic Waves*

Defined in earthquake engineering, there are two basic types of waves – body waves and surface waves. In a more detailed subdivision, body waves can be categorized into primary wave (P-wave) and secondary wave (S-wave), P-wave is a longitudinal wave like sound wave, which pushes and pulls the solid rocks; S-wave propagates in a direction perpendicular to vibration, it is transverse. Surface waves can also be divided into Love wave (L-wave) and Rayleigh wave (R-wave), the L-wave comes from the interference of S-waves and moves the ground in horizontal plan parallel with surface, while the R-wave comes from the interference between P-wave and S-wave and moves both vertically and horizontally like rolling ocean waves. Figure 3. provides a visual graph of these seismic waves and their propagation modes. In a homogenous media, the velocity of P-wave and S-wave can be described as Eq. (1) and Eq. (2) respectively 6. Surface waves travel slower than body waves and the amplitudes decrease exponentially with the depth. However, they decay slower than body waves and are most destructive because of their low frequency, long duration, and large amplitude. They travel 1 ~ 3 km/s with lots of variety within the depth of a wavelength. The wavelengths are in the order of 100m, the frequencies are about 10 ~ 30Hz 7.

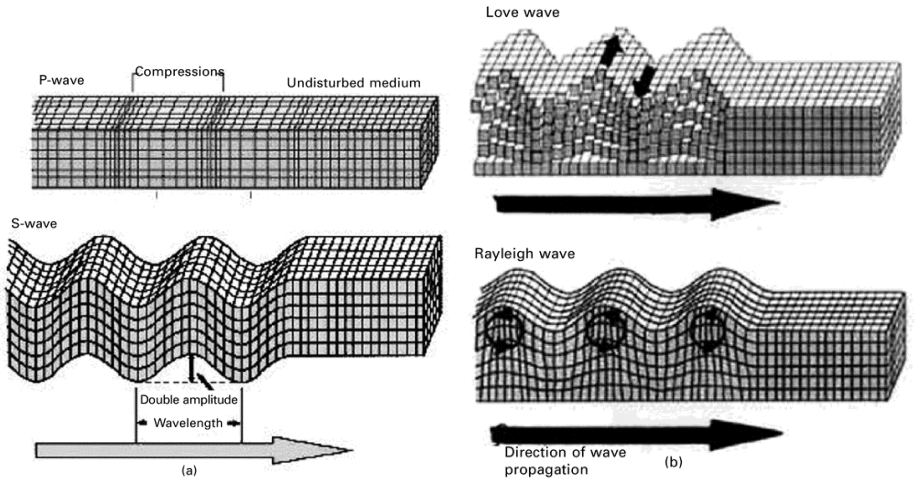

Figure 3. Sketch of (a) body waves and (b) surface waves.

$$V_p = \left(\frac{E(1+\gamma)}{\rho(1+\gamma)(1-2\gamma)} \right)^{0.5} \quad \text{Eq. (1)}$$

$$V_s = \left(\frac{E}{2\rho(1+\gamma)} \right)^{0.5} = \left(\frac{G}{\rho} \right)^{0.5} \quad \text{Eq. (2)}$$

1.3. *Mechanism of Meta-structure*

There are two basic mechanisms of the seismic meta-structures. One is to build a waveguide around the protected object, make the elastic wave propagate bypass the object without affecting it. Another is resonator, which can open a stop-band for elastic waves of certain range of frequency either by changing the effective modulus and density of the propagation medium, which, usually is the soil, or by dissipating the wave amplitude. A thorough and detailed knowledge will be presented in the case studies below.

6 Case Studies

2.1. *Cloaking Structure*

Farhat. M et al has adopted the hypothesis of Von Karman theory, obtained the out-of-plane displacement in the vertical direction is a solution of Eq. (3).

$$\langle \lambda \rangle \nabla \cdot \{ \underline{\zeta}^{-1} \nabla [\langle \lambda \rangle \nabla \cdot (\underline{\zeta}^{-1} \nabla U)] \} - \beta_0^4 U = 0, \quad \text{Eq. (3)}$$

If the cloak consists of an alternation of two homogeneous isotropic layers of thicknesses, Young's moduli and densities, an ideal cloak could be calculated with these mentioned material parameters spatially varying along

the radius. To mimic these reduced parameters, first approximate the ideal cloak by a multilayered cloak with M anisotropic homogeneous concentric layers, then approximate each layer by N thin isotropic layers through the homogenization process described. This means the overall number NM of isotropic layers can be fairly large. An original design of a cloak with 10 concentric layers of 6 materials which was numerically shown to greatly reduce forward and backward scattering for an incoming flexural plane wave ranging from 30 to 150 Hz, as shown in Figure 4. 8.

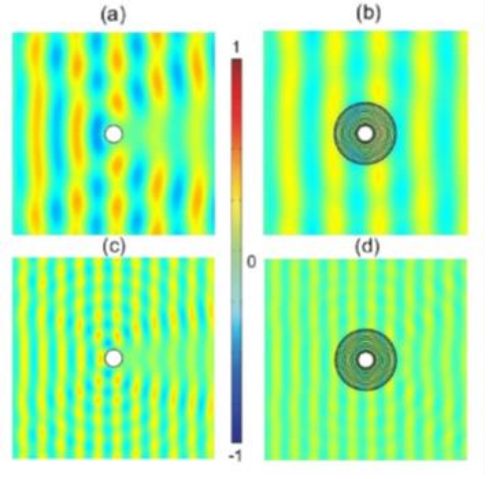

Figure 4. Real part of the displacement field scattered by a rigid clamped obstacle for an incoming plane wave of frequency 250 Hz without cloak: (a) overview, (c) closer view. While the obstacle was surrounded by a multilayered isotropic cloak: (b) overview, (d) closer view.

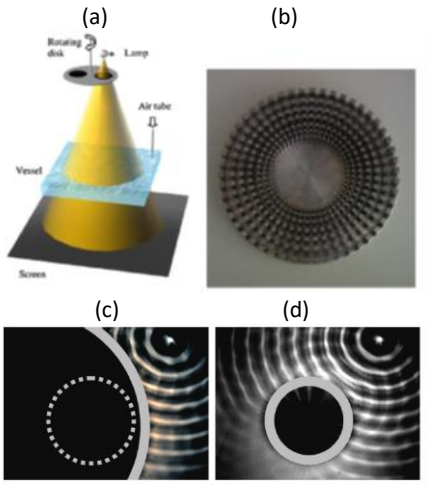

Figure 5. (a) The layout of the experiment, (b) the cloak consists of 100 rigid sectors evenly machined in a metallic ring, (c) diffraction by a rigid cylinder surrounded by the structured cloak, (d) diffraction by the rigid cylinder on its own.

Th e same research group has also designed a structured cloak based on homogenization theory, and conducted an experiment to observe the effect of cloak in a liquid **Error! Reference source not found.**. The surface waves were generated by an acoustic source, a lamp illuminated through a transparent vessel containing liquid, thus the diffraction pattern can be seen directly on the screen, as shown in Figure x. For wavelengths which are large compared with its typical heterogeneity size, the cloak behaves as an effective fluid characterized by a transversely anisotropic shear viscosity, described by Navier-Stokes equations:

$$\rho\left(\frac{\partial}{\partial t}+\mathbf{u}\cdot\nabla\right)\mathbf{u}-\mu\nabla^2\mathbf{u}=-\nabla p+\rho\mathbf{g}, \qquad \text{Eq. (4)}$$

Methoxynonafluorobutane was chosen because it is a shallow Newtonian liquid, which means a fluid which is inviscid, so that μ∇2u can be neglected outside the cloak. The fluid should be also incompressible (divergence free), irrotational (curl free) and undergo only small fluctuations around a mean vertical position (interface airliquid). The aim is to homogenize the structured cloak in order to obtain an effective anisotropic fluid described by a viscosity matrix with a large enough entry in the direction: in that case, the liquid will flow faster in the azimuthal direction, and will therefore be bent around the central region of the cloak. The results show that the wave backscattered by the rigid cylinder surrounded by the structure cloak is less apparent than that without a cloak (Figure 5.).

2.2. ***Resonator structure***

Seismic attenuator is one of the designs in this category. Kim, S. H. et al 10 made the demonstration by analog calculation. Derived from the equation of describing transverse seismic wave velocity:

$$V_s = \left(\frac{E}{2\rho(1+\gamma)}\right)^{0.5} = \left(\frac{G}{\rho}\right)^{0.5} \qquad \text{Eq. (5)}$$

If the shear modulus is negative, the velocity will become imaginary, so do the refractive index n and the wavevector. Therefore, the imaginary wavevector makes the amplitude of the seismic wave become an evanescent wave. Combining the Newton's 2nd law and continuity equation, the effective shear modulus can be expressed in the equation below:

$$\frac{1}{G_{eff}} = \frac{1}{G}\left[1 - \frac{F\omega_o^2}{\omega^2 - \omega_o^2 + i\Gamma\omega}\right] \qquad \text{Eq. (6)}$$

where ω_o is the resonance frequency and F is a geometric factor, the effective shear modulus has negative value at $1 < \omega/\omega_o < \sqrt{1+F}$.

An array of attenuator was designed (Figure 6.), and they can be placed in front of the building, as shown in Figure x. The resonance frequency can be calculated by Eq. (7)

$$\omega_o \simeq \frac{1}{\sqrt{LC}} = \sqrt{\frac{S}{l'V}}v. \qquad \text{Eq. (7)}$$

where S is the cross-section area, V is the volume, l' is the equivalent length. Actually the shape could be any form of a concrete box (cubic / hexagonal) with several side holes (Helmholtz resonator). Various kinds of resonators may cover various kinds of resonance frequencies. There happens an energy dissipation of the seismic waves inside of the waveguide and the absorbed energy will turn into sound and heat. The temperature increasing of the

waveguide depending on the magnitude of energy that arrives at the waveguide.

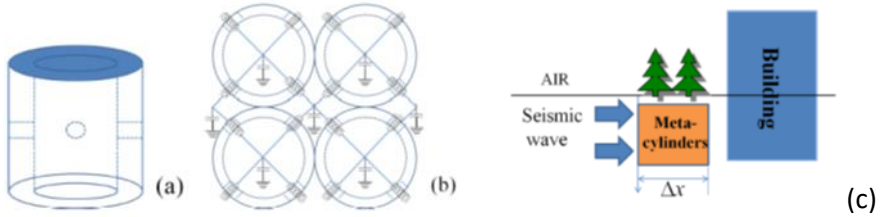

Figure 6. (a) A sample of a meta-cylinder with 4 side holes, (b) An electrical analogy of combined form of 4 meta-cylinders, (c) A vertical landscape of the metamaterial barrier and the building to protect from the seismic wave.

An in-situ experiment was carried out by Brule. S et al 11. Boreholes were drilled in the soil and sensors were placed among them (Figure 7.) As seen in the results' map x, that the dark blue region in panel has 5 times less elastic energy after carrying out the boreholes (Figure 8.).

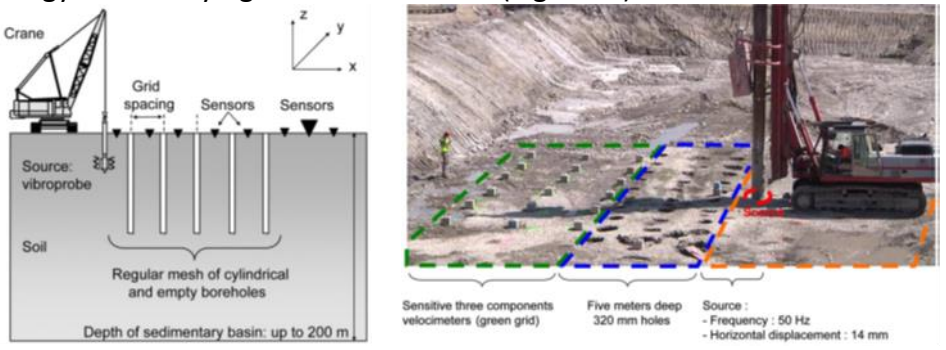

Figure 7. Schematics of the seismic testing device cross section in the x-z plane (left) and the photograph of the experiment (right).

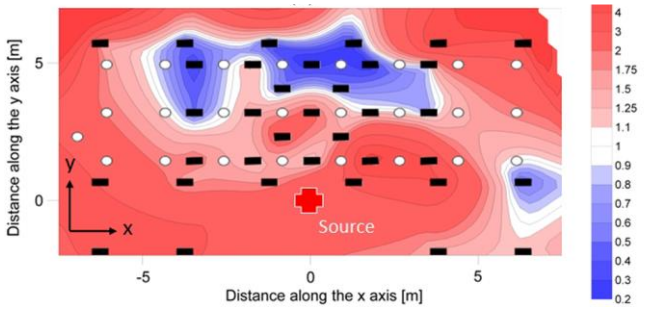

Figure 8. Ration J2/J1. J1 is the measured energy field before carrying out the boreholes, J2 is the measured energy field after carrying out the boreholes.

Another model is called isochronous mechanical oscillator, designed by Finocchio. G et al 12, which is a sphere of radius r_s constrained by the gravity to roll over a cycloidal trajectory with r_c as radius of the generating rolling circle. Despite the dynamical response of the soil near the oscillator is significantly reduced, the performances can be improved by considering an additional internal damper. It gives rise to an intrinsic phase shift between the displacements, while in the band gap, the wave continues to be evanescent. A Finite Element model with a rectangular geometry (1.25 x $1m^2$) was used. One cubic meter contains 100 internal oscillators, 25 in the x-y plane distributed in four layers along the direction of propagation of the seismic waves (z-direction, from bottom to top). The results indicate that this cubic of oscillators is able to attenuate the wave amplitude of 90%.

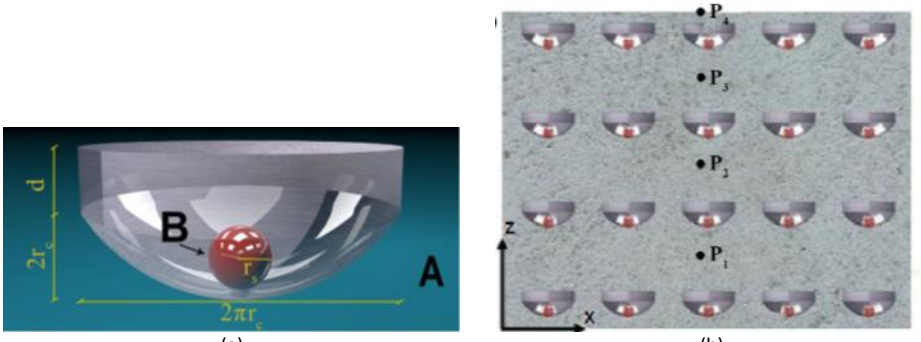

(a) (b)

Figure 9. (a) The inside structure of mechanical oscillator, (b) the rectangular geometry.

Despite those resonators in container modes, there is a new type of dissipative structure based on gyro-elastic beam, invented by Carta. G et al **Error! Reference source not found.**. The dynamic response of a single gyrobeam will cause a large number of eigenfrequencies tend to cluster within a low-frequency interval as the gyricity constant is increased. The main effect is to open a zero-frequency band-gap and to generate other stop-bands at higher frequencies. While a periodic system made of an array of elastic gyroscopic frames can contribute to new dispersion properties of waves and standing modes. Therefore, low-frequency 'energy sinks' will be created, in which waves generated by external excitations are channeled. Thus, energy is diverted away from the main structure, so it will undergo smaller displacements and smaller stresses.

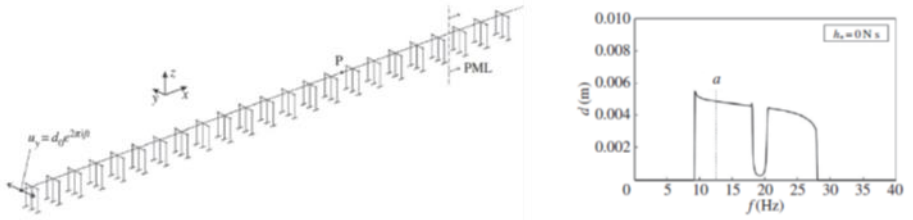

(a) (b)

Figure 10. (a) A semi-infinite gyro-elastic beam structure and (b) its response in the frequency domain (right), assuming the gyricity constant h^* =0 N s. The displacement of point P due to a harmonic displacement of amplitude d_0 =0.01 m and variable frequency f is plotted. PML are added to prevent reflections of waves at the right boundary.

7 Summary

Aseismic meta-structure is highly proposing for architectures involved with environmental security, such as nuclear reactors, oil refining complexes, power plants, dams and so on. A review of seismic metamaterials is presented containing various models and the corresponding theory. By constructing periodic arrays with certain mechanical properties and resonant frequency, the meta-structure is possible to modify the trajectory of seismic wave, or to create the band gap and turn seismic waves evanescent. Up to date, most of the concept is verified by calculation and simulation, only very few groups have conducted experiment to assess the effect. The large scale and high energy that is needed for an in-situ seismic experiment makes it more difficult to achieve than that of micro-scaled electromagnetic devices. In the future, attention is suggested to be paid not only on the development of new structures, but also on the design of experiment that can well fit the aseismic achieve under actual situation.

Acknowledgments

The author's PhD project is a part of H2020-MSCA-ITN-2017, ED-ARCHMAT (ESR1). This project has received funding from the European Union's Horizon 2020 research and innovation programme under the Marie Skłodowska-Curie grant agreement No 766311.

The theory and knowledge of metamaterials were obtained from the PhD course "01SFVRV Metamaterials Theory and multiphysics applications" in Politecnico di Torino, given by lecturer Ladislau Matekovits. Special thanks to his support and help.

References

1. Veselago, V.G. (1968). The electrodnamics of substances with simultaneously negative values of ε and μ, Soviet Physics Uspekhi 10(4), pp. 509–514.
2. Smith, D. R., Vier, D. C., Kroll, N., & Schultz, S. (2000). Direct calculation of permeability and permittivity for a left-handed metamaterial. *Applied Physics Letters*, *77*(14), 2246-2248.
3. Shelby, R. A., Smith, D. R., & Schultz, S. (2001). Experimental verification of a negative index of refraction. *science*, *292*(5514), 77-79.
4. Liu, Y., & Zhang, X. (2011). Metamaterials: a new frontier of science and technology. *Chemical Society Reviews*, 40(5), 2494-2507.
5. Carcione, J., & Cavallini, F. (1995). On the acoustic-electromagnetic analogy. *Wave motion*, *21*(2), 149-162.
6. Rajasekaran, S. (2009). *Structural dynamics of earthquake engineering: theory and application using MATHEMATICA and MATLAB*. Elsevier.
7. Villaverde, R. (2009). *Fundamental concepts of earthquake engineering*. CRC press.
8. Farhat, M., Guenneau, S., & Enoch, S. (2009). Ultrabroadband elastic cloaking in thin plates. *Physical review letters*, *103*(2), 024301.
9. Farhat, M., Enoch, S., Guenneau, S., & Movchan, A. B. (2008). Broadband cylindrical acoustic cloak for linear surface waves in a fluid. *Physical review letters*, *101*(13), 134501.
10. Kim, S. H., & Das, M. P. (2012). Seismic waveguide of metamaterials. *Modern Physics Letters B*, *26*(17), 1250105.
11. Brûlé, S., Javelaud, E. H., Enoch, S., & Guenneau, S. (2014). Experiments on seismic metamaterials: molding surface waves. *Physical review letters*, *112*(13), 133901.
12. [Finocchio, G., Casablanca, O., Ricciardi, G., Alibrandi, U., Garesci, F., Chiappini, M., & Azzerboni, B. (2014). Seismic metamaterials based on isochronous mechanical oscillators. *Applied Physics Letters*, *104*(19), 191903
13. Carta, G., Jones, I. S., Movchan, N. V., Movchan, A. B., & Nieves, M. J. (2017). Gyro-elastic beams for the vibration reduction of long flexural systems. *Proceedings of the Royal Society A: Mathematical, Physical and Engineering Sciences*, *473*(2203), 20170136.